Calculated and Measured Characteristics of a Microstrip Line Fabricated on a Y-Type Hexaferrite Substrate

Hoton How, Xu Zuo, Elwood Hokanson, Leo C. Kempel, *Senior Member, IEEE,* and Carmine Vittoria, *Fellow, IEEE*

***Abstract*—Numerical calculations have been applied to a microstrip line fabricated on a Y-type hexaferrite substrate using the Green's function technique. The formulation allows the ferrite substrate to be magnetized along an arbitrary direction. Current potentials have been used to construct the Galerkin elements and the resultant calculational scheme is applicable even when ferrimagnetic resonance is approached. Calculations compared reasonably well with measurements.**

***Index Terms*—Arbitrary magnetic bias, calculations near ferromagnetic, current-potential method, dyadic Green's function, ferrite substrate, microstrip line, Sommerfeld integral, transfer-matrix method.**

I. Introduction

ANISOTROPIC substrates, due to either the process in material preparation or crystalline asymmetry, have been used in the fabrication of microwave integrated circuits (MICs). Electromagnetic wave propagation in a ferrite substrate is also anisotropic in the presence of a dc-bias magnetic field, called the gyromagnetic effect. For the former case, the dielectric properties for wave propagation in the substrate can be described in terms of a permittivity tensor of rank 2 and, for the latter case, Polder permeability tensor results under the small-signal approximations [1]. While many authors have applied numerical calculations to microwave circuitries containing anisotropic substrates [2]–[6], in this paper, we consider wave propagation in a gyromagnetic substrate. We specifically consider the electromagnetic wave propagation in a microstrip transmission line in which the metal strip is fabricated on top of a hexaferrite substrate for which the bias magnetic field can be applied along an arbitrary direction. The formulation contained in this paper is applicable to a general stratified dielectric/magnetic structure containing circuit inhomogeneities at the interfaces. A Green's function approach is adopted in the following analysis.

In contrast to the permittivity tensor, Polder tensor elements are usually frequency dependent and exhibit strong resonance behavior with frequency and the bias magnetic field. For example, the effective permeability for wave propagation for frequencies around ferromagnetic resonance (FMR) varies from a very large positive number to a very small negative number encompassing the value zero, accompanied by a nonzero imaginary part accounting for magnetic loss [1]. Most useful magnetic microwave devices operate near FMR so that the rapid change in magnetic permeability can be effectively utilized either to obtain frequency-tuning capability or to remove the degeneracy between modes, thereby inducing nonreciprocity in wave propagation [7]. For example, ferrite phase shifters [8], resonators [9], and filters [1] are constructed according to the first principle [7], and circulators and isolators according to the second [10]. Most calculations in the past have been formulated for frequencies away from FMR in order to avoid numerical difficulties. In this paper, numerical solutions near FMR have been attempted. This was possible for us because we introduced techniques for current potentials to be discussed here.

Before solving the ac electromagnetic problem associated with a ferrite substrate, one is required to solve the dc equilibrium problem first in order to calculate the demagnetizing field due to the finite geometry of the substrate [7]. In a cubic-ferrite sample material, anisotropy is usually not important since it is small in comparison to the external bias field. In a hexaferrite substrate, the internal anisotropy field can be as large as 50 kOe and, hence, it can no longer be neglected [11]. Actually, hexaferrites are purposely introduced to alleviate [12], or even eliminate [13], the external bias field requirement at high frequencies. In a hexaferrite material, magnetic anisotropy appears in the form of an easy axis or an easy plane. For an M-type hexaferrite, the c-axis is an easy axis of magnetization, and the magnetization vector prefers to be aligned along the c-axis so as to lower its free energy [7]. For a Y-type hexaferrite, the ab-plane is an easy plane, and the magnetization vector is energetically favorable to be aligned in the ab-plane [12]. Equations (A14a) and (A14b) describe the respective effective internal fields for an easy axis and an easy plane. In this paper, we consider the substrate material to be a Y-type hexaferrite whose effective field [see (A14b)] is derived elsewhere [12].

For a given geometry, electromagnetic wave solutions arising from a point source satisfying the required (homogeneous) boundary conditions are termed Green's functions [14]. In Section II, we formulate the Green's functions of a general stratified structure containing magnetic and dielectric layers using a transverse spectral-domain analysis. For this purpose,

Manuscript received September 7, 2000; revised April 17, 2001. This work was supported by the Air Force Office of Scientific Research (Dr. A. Nachman).

H. How is with Hotech Inc., Belmont, MA 02478 USA.

X. Zuo and C. Vittoria are with the Electrical and Computer Engineering Department, Northeastern University, Boston, MA 02115 USA.

E. Hokanson is with Trans-Tech Inc., Adamstown, MD 21719 USA.

L. C. Kempel is with the Electrical and Computer Engineering Department, Michigan State University, East Lansing, MI 48824 USA.

Publisher Item Identifier S 0018-9480(02)04064-4.

we need to know *a priori* the plane-wave solutions occurring in each of the layered system. While plane-wave solutions are obvious for an isotropic dielectric layer, plane-wave solutions for an unbounded ferrite bulk magnetized along an arbitrary direction are also well known [1], whose properties are summarized in the Appendix. In general, wave propagation in a magnetized ferrite is nondegenerate, assuming different effective permeability values for different eigenmodes, resulting in different propagation speeds and polarizations.

We have applied the transfer-matrix technique to perform the transverse spectral-domain analysis [2], [6], [15]. A transfer matrix translates the surface impedance, which is itself a 2×2 matrix, from one layer interface to another, assuming the tangential components of the electromagnetic fields to be continuous across the interfaces in the absence of circuit inhomogeneities. The outermost layers are either air or a metal surface of finite conductivity, defining the (imperfect) open- or short-circuited boundaries for the layered structure, respectively. Thus, via the transfer matrices defined for the layers, these open- and/or short-circuited surface impedances are translated ultimately onto an interface containing a point source assumed by a Green's function and, after imposing the current-continuity condition at the interface position, the corresponding Green's function can, therefore, be solved.

When metal patches or strips appear in the stratified structure, as required by a microwave circuit, electromagnetic solutions can be constructed via superposition of the Green's functions. That is, electromagnetic solutions are cast in integral forms where Green's functions are superposed according to an unknown source distribution. The unknown source distribution can then be solved numerically using the Galerkin's method applied to an integral equation expressing the condition for current continuity [16]. We have used current potentials to construct the Galerkin elements and by doing so three advantages follow [17]. Not only is the symmetry of the patch/strip conserved in the calculations, but the vector Galerkin equations are also converted into scalar ones, resulting in onefold integrals for the one-dimensional (1-D) transmission-line problems and twofold integrals for the two-dimensional (2-D) metal-patch problems. Most importantly, the condition for current continuity at metal-patch/strip boundaries is automatically satisfied, forcing the normal components of the current flow to vanish at the boundaries of the metal patches/strips [18]. By using the current-potential techniques, we are able to apply numerical calculations to microstrip circuitries containing ferrite substrates even when FMR is approached. When FMR is approached, the underlying numerical problem becomes ill defined and the Galerkin elements need to be scaled to avoid large truncation errors.

As just mentioned, the resultant Galerkin elements associated with a transmission-line problem require evaluation of onefold Sommerfeld-type integrals. However, due to the fixed period (2π) of the sine and cosine functions, numerical integration at infinity is less stringent than the original Sommerfeld-type integrals containing oscillations of Bessel functions at infinity [16]. As such, extrapolation schemes have been applied to evaluate the integrals at infinity.

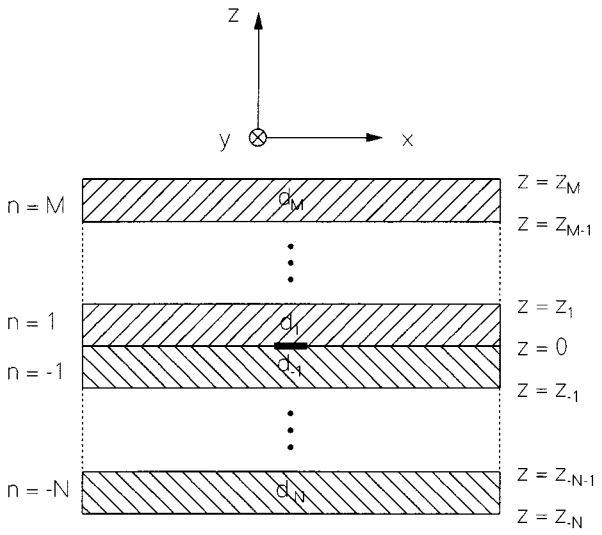

Fig. 1. Geometry of a stratified structure containing multiple layers. A planar circuit is located at the $z = 0$ plane.

Experimentally, we have fabricated a microstrip transmission line on a Y-type hexaferrite substrate exhibiting a magnetic easy plane [12]. While the significance of a magnetic easy plane is discussed in a separate paper [12], numerical calculations for wave propagation along a microstrip line involving a magnetic easy plane implied by a Y-type hexaferrite substrate follow in this paper. Calculations compared reasonably well with measurements.

II. Formulation

We present a general formulation that a planar microwave circuit is embedded in a stratified structure involving dielectric/magnetic layers as substrates/superstrates. This is shown in Fig. 1. The planar circuit is located at $z = 0$ and there are M layers in the $+z$-direction and N layers in the $-z$-direction. We denote z as the direction normal to the layered structure. The thickness of the νth layer is d_ν, $M \geq \nu \geq -N$. In Fig. 1, the outermost surfaces are either a metal boundary of finite conductivity σ or air. The following formulation allows the boundary conditions at the outermost surfaces $z = z_M$ and $z = z_{-N}$ to be translated onto the interface at $z = 0$ containing the microwave circuit, admitting a 2-D analysis there. For this purpose, we have adopted the so-called transfer-matrix technique [2], [6], [15]. Although the present analysis considers only one single plane that contains the circuit inhomogeneity, the same analysis can be generalized so that more than one planar circuits may appear at several layer interfaces. In Fig. 1, the resultant electromagnetic wave solutions in the presence of a vertical point dipole is termed as the dyadic Green's function [16].

The transfer-matrix method is applied in the spectral domain. A transfer matrix is a 4×4 matrix and, for a given transverse spectral vector $\underline{\mathbf{k}}_t = (k_x \;\; k_y)^T$, it correlates the tangential components of the RF e- and h-fields on both sides of a layer [see (3)]. Here, the superscript T denotes transposition of a row

vector into a column vector. Thus, for the νth layer the transfer matrix can be written as

$$\underline{\underline{\boldsymbol{T}}}_{\nu}(d_{\nu}) = \underline{\underline{\Gamma}}_{\nu}(z_{\nu+1}) \cdot \underline{\underline{\Gamma}}_{\nu}^{-1}(z_{\nu}) \tag{1}$$

with (2), shown at the bottom of this page, so that

$$\begin{pmatrix} e_x(z_{\nu+1}) \\ e_y(z_{\nu+1}) \\ h_x(z_{\nu+1}) \\ h_y(z_{\nu+1}) \end{pmatrix} = \underline{\underline{\boldsymbol{T}}}_{\nu}(d_{\nu}) \cdot \begin{pmatrix} e_x(z_{\nu}) \\ e_y(z_{\nu}) \\ h_x(z_{\nu}) \\ h_y(z_{\nu}) \end{pmatrix}. \tag{3}$$

In (2), $k_{\nu\alpha z}$, $M \geq \nu \geq -N$, and $4 \geq \alpha \geq 1$ denotes the z-component of the wave vector of the αth eigenmode in the νth layer satisfying

$$k_x^2 + k_y^2 + k_{\nu\alpha z}^2 = \epsilon_{\nu\alpha}\mu_{\nu\alpha}(\omega/c)^2. \tag{4}$$

In (4), $\epsilon_{\nu\alpha}$ and $\mu_{\nu\alpha}$ are the dielectric constant and permeability of the αth eigenmode in the νth layer, ω is the angular frequency, c the speed of light in vacuum, and Gaussian units have been used throughout this analysis.

For an isotropic medium, (4) reduces to the regular dispersion relation for wave propagation, and $\epsilon_{\nu\alpha}$ and $\mu_{\nu\alpha}$ are all degenerate, i.e., α independent, denoting the permittivity and permeability of the medium, respectively. For an anisotropic medium, the four eigenmodes become nondegenerate, assuming different values for permittivity and/or for permeability $\epsilon_{\nu\alpha}$ and $\mu_{\nu\alpha}$, $\alpha = 1,2,3,4$. The procedure for solving the nondegenerate dispersion relation of a gyromagnetic medium is given in the Appendix. That is, when k_x, and k_y are given, $k_{\nu\alpha z}$ is solved from (A5). Since (A5) is a quartic equation, there are four eigenmodes, corresponding to the four solutions of $k_{\nu\alpha z}$. Equation (4) then solves for $\mu_{\nu\alpha}$, denoting the effective permeability of the αth mode, which is used to express the electromagnetic fields of the αth eigenmode given in (A20)–(A28). The permittivity of the eigenmodes are all the same, $\epsilon_{\nu\alpha} = \epsilon_d$, $\alpha = 1,2,3,4$, where ϵ_d denotes the dielectric constant of the ferrite layer. More details about the solution of the eigenmodes can be found in the Appendix as related to (A5).

We note in the limit of a transversely applied magnetic bias field the coefficients $P_3 = P_1 = 0$ [see (A7) and (A8)] since $e_{nz} = 0$. Thus, (A5) implies two doubly degenerate eigenmode pairs, as derived in [6]. It can be shown that (A5) reduces to the corresponding equations in [6] for a transversely applied bias field. However, if the bias field is along an arbitrary direction, (A5) predicts, in general, four nondegenerate eigenmodes. We note that FMR occurs if the coefficient $P_4 = 0$ [see (A6)]. At FMR, (A5) implies an incomplete set of eigenmodes, which spans a vector space with dimensionality smaller than required by the present spectral-domain analysis or the transfer matrix techniques [see (1)].

The tangential components of the e and h-fields associated with the αth eigenmode in the νth layer are expressed as $(e_{\nu\alpha x} \;\; e_{\nu\alpha y})^T$ and $(h_{\nu\alpha x} \;\; h_{\nu\alpha y})^T$ in (2), respectively. The Γ-matrices and, hence, the transfer matrices $\underline{\underline{\boldsymbol{T}}}_{\nu}(d_{\nu})$ for a dielectric layer and for a ferrite layer [see (2)] are given in the Appendix. The index ν has been dropped in the Appendix for reasons of clarity.

The surface impedance matrix $\underline{\underline{\boldsymbol{Z}}}(z)$ can be defined as follows:

$$\begin{pmatrix} e_x(z) \\ e_y(z) \end{pmatrix} = \underline{\underline{\boldsymbol{Z}}}(z) \cdot \begin{pmatrix} h_x(z) \\ h_y(z) \end{pmatrix} \tag{5}$$

where the dependence of the quantities in (5), say, e_x, e_y, h_x, h_y, and $\underline{\underline{\boldsymbol{Z}}}$ on k_x and k_y is understood. Thus, when a transfer matrix is defined to translate the tangential components of the RF electromagnetic fields over one layer thickness [see (3)], the surface impedance will also be transferred according to the following equation:

$$\underline{\underline{\mathbf{Z}}}(z_{\nu+1}) = \left[\underline{\underline{\mathbf{a}}}_{\nu}\underline{\underline{\mathbf{Z}}}(z_{\nu}) + \underline{\underline{\mathbf{b}}}_{\nu}\right]\left[\underline{\underline{\mathbf{c}}}_{\nu}\underline{\underline{\mathbf{Z}}}(z_{\nu}) + \underline{\underline{\mathbf{d}}}_{\nu}\right]^{-1} \tag{6}$$

where $\underline{\underline{\mathbf{a}}}_{\nu}$, $\underline{\underline{\mathbf{b}}}_{\nu}$, $\underline{\underline{\mathbf{c}}}_{\nu}$, and $\underline{\underline{\mathbf{d}}}_{\nu}$ are the 2×2 partition matrices of $\underline{\underline{\mathbf{T}}}_{\nu}$ given by

$$\underline{\underline{\boldsymbol{T}}}_{\nu} = \begin{pmatrix} \underline{\underline{\boldsymbol{a}}}_{\nu} & \underline{\underline{\boldsymbol{b}}}_{\nu} \\ \underline{\underline{\boldsymbol{c}}}_{\nu} & \underline{\underline{\boldsymbol{d}}}_{\nu} \end{pmatrix}. \tag{7}$$

Since, except at $z = 0$, the tangential components of the e- and h-fields are continuous across layer interfaces, the transfer matrices can be multiplied together to provide an overall transformation relating the outermost boundaries of the structure to the $z = 0$ plane. Thus, we define two overall transfer matrices, top and bottom, denoted as $\underline{\underline{\mathbf{T}}}_t$ and $\underline{\underline{\mathbf{T}}}_b$, respectively, as

$$\underline{\underline{\mathbf{T}}}_t = \left[\underline{\underline{\mathbf{T}}}_M \cdots \underline{\underline{\mathbf{T}}}_2\underline{\underline{\mathbf{T}}}_1\right]^{-1} \tag{8}$$

$$\underline{\underline{\mathbf{T}}}_b = \underline{\underline{\mathbf{T}}}_{-N} \cdots \underline{\underline{\mathbf{T}}}_{-2}\underline{\underline{\mathbf{T}}}_{-1} \tag{9}$$

such that

$$\begin{pmatrix} e_x(0^+) \\ e_y(0^+) \\ h_x(0^+) \\ h_y(0^+) \end{pmatrix} = \underline{\underline{\boldsymbol{T}}}_t \cdot \begin{pmatrix} e_x(z_M) \\ e_y(z_M) \\ h_x(z_M) \\ h_y(z_M) \end{pmatrix}$$

$$\begin{pmatrix} e_x(0^-) \\ e_y(0^-) \\ h_x(0^-) \\ h_y(0^-) \end{pmatrix} = \underline{\underline{\boldsymbol{T}}}_b \cdot \begin{pmatrix} e_x(z_{-N}) \\ e_y(z_{-N}) \\ h_x(z_{-N}) \\ h_y(z_{-N}) \end{pmatrix}. \tag{10}$$

$$\underline{\underline{\Gamma}}_{\nu}(z) = \begin{pmatrix} e_{\nu 1x}\exp(ik_{\nu 1z}z) & e_{\nu 2x}\exp(ik_{\nu 2z}z) & e_{\nu 3x}\exp(ik_{\nu 3z}z) & e_{\nu 4x}\exp(ik_{\nu 4z}z) \\ e_{\nu 1y}\exp(ik_{\nu 1z}z) & e_{\nu 2y}\exp(ik_{\nu 2z}z) & e_{\nu 3y}\exp(ik_{\nu 3z}z) & e_{\nu 4y}\exp(ik_{\nu 4z}z) \\ h_{\nu 1x}\exp(ik_{\nu 1z}z) & h_{\nu 2x}\exp(ik_{\nu 2z}z) & h_{\nu 3x}\exp(ik_{\nu 3z}z) & h_{\nu 4x}\exp(ik_{\nu 4z}z) \\ h_{\nu 1y}\exp(ik_{\nu 1z}z) & h_{\nu 2y}\exp(ik_{\nu 2z}z) & h_{\nu 3y}\exp(ik_{\nu 3z}z) & h_{\nu 4y}\exp(ik_{\nu 4z}z) \end{pmatrix} \tag{2}$$

The relationship between the two column vectors $(e_x(0^+)e_y(0^+)h_x(0^+)h_y(0^+))^T$ and $(e_x(0^-)e_y(0^-)h_x(0^-)\ h_y(0^-)\ )^T$ is determined from the boundary conditions imposed by the planar circuit at $z = 0$, as connected together by the use of the dyadic Green's functions discussed below. We note that while transfer matrices are multiplied together translating the tangential components of the electromagnetic fields across layers, as described by (8) and (9), the transformation of surface impedance defined by the functional form of (6) also multiplies or compounds as a consequence of the translation process. This is indeed true since transformation of (6) is an isomorphic representation of the transfer matrix $\underline{\underline{\mathbf{T}}}_\nu$ under the operation of matrix multiplication. Therefore, we have

$$\underline{\underline{\mathbf{Z}}}(0^+) = \left[\underline{\underline{\mathbf{a}}}_t\underline{\underline{\mathbf{Z}}}(z_M) + \underline{\underline{\mathbf{b}}}_t\right]\left[\underline{\underline{\mathbf{c}}}_t\underline{\underline{\mathbf{Z}}}(z_M) + \underline{\underline{\mathbf{d}}}_t\right]^{-1} \tag{11}$$

$$\underline{\underline{\mathbf{Z}}}(0^-) = \left[\underline{\underline{\mathbf{a}}}_b\underline{\underline{\mathbf{Z}}}(z_{-N}) + \underline{\underline{\mathbf{b}}}_b\right]\left[\underline{\underline{\mathbf{c}}}_b\underline{\underline{\mathbf{Z}}}(z_{-N}) + \underline{\underline{\mathbf{d}}}_b\right]^{-1} \tag{12}$$

where $\underline{\underline{\mathbf{a}}}_t$, $\underline{\underline{\mathbf{b}}}_t$, $\underline{\underline{\mathbf{c}}}_t$, and $\underline{\underline{\mathbf{d}}}_t$ denote the partition matrices associated with the top transfer matrix, e.g., $\underline{\underline{\mathbf{T}}}_t$.

Now we need to know the surface impedance of the outermost surfaces. We consider the surface impedances $\underline{\underline{\mathbf{Z}}}(z_M)$ and $\underline{\underline{\mathbf{Z}}}(z_{-N})$ to be those associated with either a short-circuited metal ground plane or an open-circuited half-space filled with, say, air. For a short-circuited ground plane, the surface impedance can be derived as

$$\underline{\underline{\boldsymbol{Z}}}_s = \pm\left[\frac{c}{4\pi}\right]\frac{1-i}{\sigma\delta}\begin{pmatrix} 0 & 1 \\ -1 & 0\end{pmatrix} \tag{13}$$

and for an open-circuited half-space

$$\underline{\underline{\boldsymbol{Z}}}_o = \pm\begin{pmatrix} e_{Ax} & e_{Bx} \\ e_{Ay} & e_{By}\end{pmatrix}\begin{pmatrix} 0 & \sqrt{\dfrac{\mu_o}{\epsilon_o}} \\ -\sqrt{\dfrac{\mu_o}{\epsilon_o}} & 0\end{pmatrix}\begin{pmatrix} e_{Ax} & e_{Bx} \\ e_{Ay} & e_{By}\end{pmatrix}^{-1} \tag{14}$$

where the $+(-)$ sign applies if the surface being considered possesses an upward (downward) surface normal. In (13), σ denotes the electrical conductivity of the metal plane, and $\delta = c(2\pi\omega\sigma)^{-1/2}$ is the skin depth. In (14), ϵ_o and μ_o are the dielectric constant and magnetic permeability of the open space, which may differ from one if material other than air is used in filling the half-space. The column vectors $\underline{\mathbf{e}}_A = (e_{Ax}\ e_{Ay})^T$ and $\underline{\mathbf{e}}_B = (e_{Bx}\ e_{By})^T$ are defined in (A1) and (A2). Thus, once the surface impedances $\underline{\underline{\mathbf{Z}}}(z_M)$ and $\underline{\underline{\mathbf{Z}}}(z_{-N})$ are given from (13) or (14). $\underline{\underline{\mathbf{Z}}}(0^+)$ and $\underline{\underline{\mathbf{Z}}}(0^-)$ can then be calculated from (11) and (12) provided that all of the transfer matrices $\underline{\underline{\mathbf{T}}}_\nu$, $M \geq \nu \geq -N$ are known *a priori* [see (7) and (8)]. Note that the present formulation encompasses losses of all kinds, including dielectric loss [see (A4) and (A15)], magnetic loss [see (A14a) and (A14b)], and conductor loss [see (13) and (17)]; radiation-wave loss presents in (14) and surface-wave loss is inherent to the Green's function construction contained in the transfer matrices $\underline{\underline{\mathbf{T}}}_t$ and $\underline{\underline{\mathbf{T}}}_b$ [see (8) and (9)].

Let $\underline{\underline{\mathbf{G}}}(k_x, k_y)$ be the Green's function dyad in the spectral domain denoting the tangential electric field generated by a point-dipole source located at the $z = 0$ interface. That is, for a given current distribution in the interface $\underline{\boldsymbol{j}}(x', y')$, the generated tangential electric field at $z = 0$ is

$$\begin{aligned}\underline{\boldsymbol{e}}_t(x, y) = \frac{1}{4\pi^2}\int_{-\infty}^{\infty}dk_x\int_{-\infty}^{\infty}dk_y\int_{-\infty}^{\infty}dx'\int_{-\infty}^{\infty}dy' \\ \cdot\exp\left[ik_x(x-x')\right]\exp\left[ik_y(y-y')\right] \\ \cdot\underline{\underline{\boldsymbol{G}}}(k_x, k_y)\underline{\boldsymbol{j}}(x', y').\end{aligned} \tag{15}$$

From Ampere's law, the Green's function dyad is

$$\begin{aligned}\underline{\underline{\boldsymbol{G}}}(k_x, k_y) = \left\{\left[\underline{\underline{\boldsymbol{Z}}}(0^+; k_x, k_y)\right]^{-1} - \left[\underline{\underline{\boldsymbol{Z}}}(0^-; k_x, k_y)\right]^{-1}\right\}^{-1} \\ \cdot\begin{pmatrix} 0 & 1 \\ -1 & 0\end{pmatrix}.\end{aligned} \tag{16}$$

In (15), both the source point $(x'\ y')$ and the observation point $(x\ y)$ are located at $z = 0$. The integral equation to solve is [16], [17]

$$\underline{\boldsymbol{e}}_t(x, y) + Z_s\underline{\boldsymbol{j}}(x, y) = \underline{\boldsymbol{E}}_c(x, y) \tag{17}$$

where

$$Z_s = (1-i)(\omega/8\pi\sigma)^{1/2} \tag{18}$$

denotes the surface impedance, σ denotes the conductivity of the metal patch at $z = 0$, and $\underline{\boldsymbol{E}}_c$ denotes the tangential component of the electric field generated by the excitation current or the feeder-line current.

In this paper, we consider the microstrip solutions for which wave propagates along the y-direction without imposing to external-current excitation $\underline{\boldsymbol{E}}_c = 0$ in (17). That is, we are considering the normal-mode solutions intrinsic to a microstrip transmission line. Under these considerations, (15) and (17) are combined to yield

$$\begin{aligned}\frac{1}{2\pi}\int_{-\infty}^{\infty}dk\int_{-\infty}^{\infty}dx'\exp\left[ik(x-x')\right]\underline{\underline{\boldsymbol{G}}}(k, \beta)\underline{\boldsymbol{j}}(x') \\ - Z_s\underline{\boldsymbol{j}}(x) = 0.\end{aligned} \tag{19}$$

Here, for clarity, we have used different symbols k and β for k_x and k_y, respectively. The homogeneous equations [i.e., (19)] are then solved numerically, giving rise to the dispersion relation expressing the wave propagation constant β as a function of the angular velocity ω.

The microstrip geometry is depicted in Fig. 2, where the metal strip is of width w, lying on the $z = 0$ plane, extending from $x = 0$ to $x = w$. Following [16] and [17], we express the current distribution in the metal strip in terms of a current basis $\{\underline{\boldsymbol{j}}_m\}$

$$\underline{\boldsymbol{j}}(x, y) = \sum_{m=0}^{\infty}a_m\underline{\boldsymbol{j}}_m(x, y) \tag{20}$$

where the current elements $\{\underline{\boldsymbol{j}}_m\}$ are derived from current potentials as

$$\underline{\boldsymbol{j}}_m(x, y) = \underline{\nabla}_t\left[\cos(m\pi x/w)e^{i\beta y}\right], \qquad m = 0, 1, 2, \ldots. \tag{21}$$

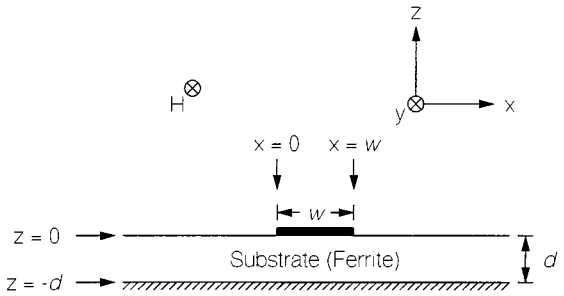

Fig. 2. Geometry of the microstrip line fabricated on a Y-type hexaferrite substrate.

Here, $\underline{\nabla}_t$ denotes the two-dimensional transverse gradient operator. Note that the normal components of the current elements vanish at the microstrip edges, as required by the current continuity equation [18]. By using the Galerkin's method the Galerkin elements associated with (19) are

$$\begin{aligned} A_{mn} &= \frac{1}{2\pi}\int_{-\infty}^{\infty} dk \int_0^w dx \int_0^w dx' e^{ik(x-x')} \underline{\boldsymbol{j}}_m(x')^+ \\ &\quad \cdot \underline{\underline{\boldsymbol{G}}}(k,\beta)\underline{\boldsymbol{j}}_n(x) + Z_s \int_0^w dx \underline{\boldsymbol{j}}_m(x)^+ \underline{\boldsymbol{j}}_n(x) \\ &= \frac{1}{2\pi}\int_{-\infty}^{\infty} dk \left\{ \left(\frac{m\pi}{w}\right)^2 \left(\frac{n\pi}{w}\right)^2 G_{11} \right. \\ &\qquad + \beta k \left[\left(\frac{m\pi}{w}\right)^2 G_{12} + \left(\frac{n\pi}{w}\right) G_{21} \right] \\ &\qquad \left. + \beta^2 k^2 G_{22} \right\} \\ &\quad \cdot \frac{\left[e^{i(kw+m\pi)}+1\right]\left[-e^{-i(kw+n\pi)}+1\right]}{\left[k^2-(m\pi/w)^2\right]\left[k^2-(n\pi/w)^2\right]} \\ &\quad + \delta_{mn}\frac{w}{2}\left[\left(\frac{m\pi}{w}\right)^2 + \beta^2\right] Z_s \end{aligned} \tag{22}$$

where δ_{mn} denotes the delta–Kronecker function and the dagger $+$ denotes adjoint operation. By setting the determinant of the Galerkin matrix (A_{mn}) into 0, the dispersion relation for wave propagation is determined, expressing the propagation constant β as a function of the angular velocity ω. In calculating the Galerkin elements, twofold integrations have been carried out analytically and it is only required to evaluate a onefold integration numerically [see (22)].

By employing the current potentials, the Galerkin equation has been reduced from vector form (19) to scalar form (22). Symmetry retains in the calculations for Galerkin elements. For example, in isotropic media, the left–right symmetry of the microstrip geometry implies that we need only to evaluate even-numbered elements, i.e., m and n are even numbers in (22). Also, integration for k from $-\infty$ to 0 in (22) is the same as from 0 to ∞ since wave propagation is reciprocal due to the mirror symmetry of the circuit. However, in an anisotropic medium, say, a ferrite, the presence of a bias magnetic field removes these symmetries. As a result, microstrip currents are shifted onto one side of the metal strip, known as the field displacement effect in the literature [1]. Wave propagation becomes nonreciprocal since the mirror symmetry no longer holds due to the presence of the bias magnetic field or the anisotropy field.

III. Results

Similar to the original Sommerfeld integrals, surface modes appear, due to poles in the integrand of (22). We note that the lateral strip-resonant modes, occurring at $k = \pm m\pi$ and $\pm n\pi$, are actually not poles of the integrand since, at these wave numbers, the numerator of the integrand also vanishes, appearing as first-order zeros. The same results occur for other metal patch geometries, as illustrated in [16] and [17]. Numerical techniques evaluating Sommerfeld-type integrals are discussed in [16] and [17], and most techniques still apply here. However, due to the fixed period of the integrand at infinity, say, 2π, integration of these integrands can be carried out using an extrapolation scheme.

Due to losses of various kinds, surface poles are pushed off from the real k-axis, allowing the integrals to be evaluated numerically. However, sharp cancellation occurs near surface poles and the integration processes need to be handled with care [16], [17]. In performing numerical integrations, we define a cutoff for the wavenumber k. Integration from $-$cutoff to $+$cutoff is accomplished using the implicit fifth-order Runge–Kutta method, which is able to monitor local truncation errors to adaptively adjust step size to ensure the overall integration accuracy [19]. Integrations from $-\infty$ to $-$cutoff and from cutoff to ∞ are then evaluated using the extrapolation scheme. Initial value for cutoff is set to be 100 $(\omega/c)\epsilon_f^{1/2}$. This cutoff value is then doubled to check the overall accuracy. This process continues until the required tolerance is met.

Calculations of Galerkin elements have been carried out retaining six significant digits when outside the FMR region. When FMR is approached, the Galerkin matrix becomes ill behaved. We have to scale the matrix elements properly to avoid numerical underflow and to avoid large truncation errors. FMR region is defined for $\omega_K < \omega < \omega_{\mathrm{FMAR}}$, and ω_K and ω_{FMAR} are the Kittel frequency and ferromagnetic antiresonant frequency given by [12, eqs. (7) and (8)], respectively. In the following calculations, we have used 20 Galerkin elements. Once the wavenumber β is solved as the lowest zero of the eigenvalues, the fundamental mode, the unknown current expansion coefficient a_m, $m = 0, 1, 2, 3, \ldots$ [see (20)] are determined as the associated eigenvector.

Impedance of a transmission line supporting TEM-like wave propagation can be defined as

$$Z_L = V/I \tag{23}$$

where V is the voltage drop across the central conductor and ground plane and I is the current flowing at the central conductor. For the microstrip line shown in Fig. 2, I can be calculated as

$$I = \int_0^w dx j_Y = i\beta a_0 \tag{24}$$

and V can be calculated from

$$\begin{aligned} V = \frac{1}{2\pi}\int_{-\infty}^{\infty} dk \int_0^w dx' \int_w^{\infty} dx e^{ik(x-x')} \begin{pmatrix} 1 \\ 0 \end{pmatrix}^T \\ \cdot \underline{\underline{\boldsymbol{G}}}(k,\beta)\underline{\boldsymbol{j}}_m(x'). \end{aligned} \tag{25}$$

From (23), we obtain

$$Z_L = \frac{1}{2\pi\beta}\sum_{m=0}^{\infty}\left(\frac{a_m}{a_0}\right)\int_{-\infty}^{\infty} dk\,\frac{e^{ikw}}{k}\left[\left(\frac{m\pi}{w}\right)^2 G_{11} + \beta k G_{12}\right] \cdot \frac{1-e^{-i(kw-m\pi)}}{k^2-(m\pi/w)^2}. \quad (26)$$

In (25), in calculating the voltage drop, we have chosen the integration path to be along $w < x < \infty$ and $z = 0$. As can be verified from Faraday's law, this voltage drop is independent of the integration path connecting the central conductor with the ground plane so long as the longitudinal component of the RF h-field is negligible comparing to the transverse components, i.e., $h_y \ll h_x$ or h_z. Otherwise, the concept of line impedance does not make much sense. Here, we also assume the strip is made of good conductor so that voltage drop across the metal strip is negligible. It can be proven that, for a transmission line supporting TEM-like waves, the definition for line impedance [see (23)] is equivalent to

$$Z_L = 2P/I^*I \quad (27)$$

where P is the power delivered by the transmission line.

Under transmission measurement, a transmission line of length ℓ, impedance Z_L, and wave propagation constant β is connected with probes at two ends of standard impedance $Z_o = 50\ \Omega$, or $Z_o = 4\pi/c$, which is expressed in Gaussian unit. The transmission coefficient is

$$\tau = \frac{2Z_oZ_L}{2Z_oZ_L\cos\beta L - i\left(Z_o^2+Z_L^2\right)\sin\beta L} \quad (28)$$

and the reflection coefficient is

$$\rho = \frac{-i\left(Z_O^2-Z_L^2\right)\sin\beta L}{2Z_oZ_L\cos\beta L - i\left(Z_o^2+Z_L^2\right)\sin\beta L}. \quad (29)$$

Experimentally, we have fabricated a microstrip transmission line using a single-crystal Y-type hexaferrite as the substrate material [12]. The composition of the substrate material is $Ba_2MgZnFe_{12}O_{22}$ and the easy plane coincides with the substrate surfaces, i.e., the xy-plane. The hexaferrite substrate material was characterized using a vibrating sample magnetometer (VSM) to show a saturation magnetization $4\pi M_S = 2.86$ kg, and an anisotropy field $H_A = 7.94$ kOe. The fabricated microstrip line is characterized by the following parameters: thickness $d = 0.010$ in, width $w = 0.0051$ in, length $\ell = 4$ mm, and dielectric constant $\epsilon_f = 18$. The dielectric loss tangent $\tan\delta_f$ was assumed to be 0.01 and FMR linewidth $\Delta H = 100$ Oe. Other properties of the fabricated microstrip line, as well as measurements, can be found in [12].

Fig. 3 shows the calculated current profile of the longitudinal current $j_y(x)$ and the transverse current $j_x(x)$ plotted over the width of the metal strip, assuming the external field $H_o = 5$ kOe, and the frequency $f = 20$ GHz. It is seen in Fig. 3 that current distribution is slightly asymmetric with respect to the center of the strip, showing the field displacement effect due to the presence of a bias magnetic field. Longitudinal currents are crowded at the edges of the strip at which positions the transverse current vanishes, as expected.

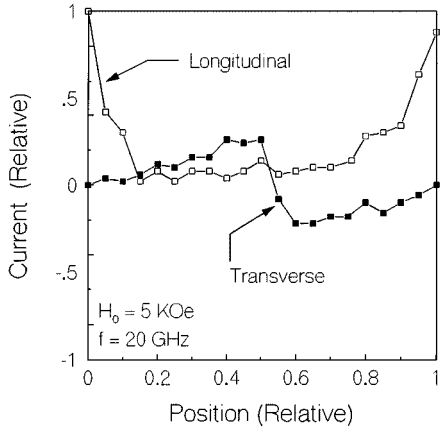

Fig. 3. Calculated current profile for the longitudinal and transverse components across the strip width of the fabricated microstrip line.

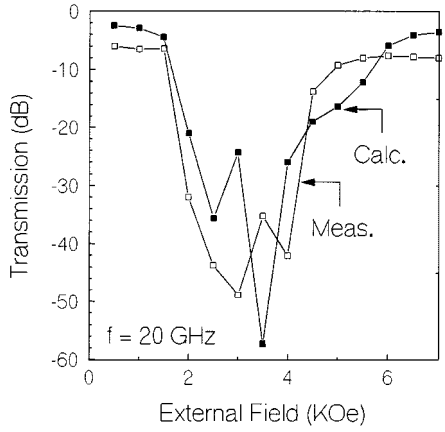

Fig. 4. Calculated and measured transmission amplitude at 20 GHz, plotted as a function of the external bias field.

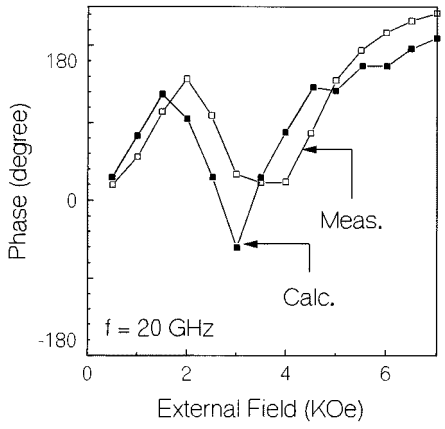

Fig. 5. Calculated and measured transmission phase at 20 GHz, plotted as a function of the external bias field.

Figs. 4 and 5 plot the calculated and measured transmission coefficient for the amplitude and phase, respectively, assuming the frequency $f = 20$ GHz. In Fig. 4, the measured insertion loss is larger than calculated even outside the FMR region. Reasons for this may be that the dielectric loss tangent and FMR linewidth assumed by the calculations are smaller than their actual values, corresponding to electric and magnetic losses, respectively. Other losses, for example, discontinuity resulted

from the coax-microstrip adapters employed under transmission measurements, may also partially explain the discrepancy. Discrepancy between theory and calculations in the FMR region is even bigger due to the difficulty in obtaining good numerical accuracy in that region. Also, the impedance value calculated by using (26) may not be adequate in the FMR region since, to large extent, wave propagation is no more TM-like. Measurements show that wave propagation in the fabricated microstrip line is roughly reciprocal, especially when outside the FMR region.

The calculated transmission phase basically confirms measurements (Fig. 5) showing a resonant structure when FMR comes across. Of special notice, it is seen in Fig. 5 that phase shift occurs linearly in the low field region prior to FMR, suggesting that a transmission line involving Y-type hexaferrite material is a superior candidate for phase shifters, especially at high frequencies. For a Y-type hexaferrite material, the crystalline anisotropy can be effectively used to substitute, at least partially, the bias field requirement. For example, in the absence of a material anisotropy, an external field in the order of 7 kOe is required to effectively change the phase of a microwave signal at 20 GHz. Similarly, an M-type hexaferrite can also provide an internal field along the easy axis, thereby alleviating the bias field requirement. However, in using an M-type hexaferrite, it is inevitable to introduce a demagnetizing field in the order of $4\pi M_s$ [see (A14a)] and, hence, it is not favorable for practical applications, at least as phase shifters. M-type hexaferrite have been practically used to fabricate self-biased circulators at millimeter-wave frequencies [7].

IV. Conclusions

We conclude that Green's function calculations utilizing the current-potential technique provide sufficient accuracy in calculating a layered structure containing anisotropic ferrite substrates/superstrates magnetized along an arbitrary direction. Our calculations are applicable even when the region of FMR is approached. The formulation may be generalized to include circuit inhomogeneities at multiple interfaces. For a transmission-line like geometry, the calculations are 1-D, and for a antenna-patch-like geometry the calculations are 2-D. However, if the finite lateral dimension is considered important, one needs to revert to a full-wave three-dimensional (3-D) analysis invoking generic numerical routines for finite-element and finite-difference calculations. The fit between our calculated and measured phase shift and amplitude as a function of the bias field is reasonable in view of the fact that there were no adjustable parameters. All parameters used in the calculations were obtained directly from measurements, including dc, VSM, and FMR measurements [12].

Appendix

For clarity, the layer index ν is dropped in the following discussion. For an isotropic dielectric medium, the four eigenmodes are degenerate so that $\epsilon_1 = \epsilon_2 = \epsilon_3 = \epsilon_4 = \epsilon_d$ and $\mu_1 = \mu_2 = \mu_3 = \mu_4 = 1$. Here, ϵ_d denotes the dielectric constant of the medium. The longitudinal wave propagation constant k_z can thus be calculated from (4) for $\alpha = 1, 2, 3$, and 4. Denote the azimuthal and polar angles of the column vector $\underline{\mathbf{k}} = (k_x \;\; k_y \;\; k_z)^T$ as ϕ and θ, respectively. We define two column vectors

$$\underline{\mathbf{e}}_A = (1-\Big(1-\cos\theta)\cos^2\phi-(1-\cos\theta)\sin\phi\cos\phi\Big)^T \quad \text{(A1)}$$

$$\underline{\mathbf{e}}_B = (-\Big(1-\cos\theta)\sin\phi\cos\phi 1-(1-\cos\theta\Big)\sin^2\phi)^T \quad \text{(A2)}$$

from which the Γ-matrix [see (2)] can be written as shown in (A3) at the bottom of this page. In (A3), we have defined the wave impedance of the medium as $\zeta = \epsilon_d^{-1/2}$. In order to take into account dielectric loss, the dielectric constant ϵ_d shall be replaced by a complex number whose imaginary part is proportional to the dielectric loss tangent of the medium $\tan\delta_d$

$$\epsilon_d \to \epsilon_d(1 + i\tan\delta_d). \quad \text{(A4)}$$

For a ferrite medium biased by a dc magnetic field along an arbitrary direction, the four eigenmodes for wave propagation are, in general, nondegenerate [1]. Instead of using (4), the longitudinal wave number k_z can now be solved from the following quartic equation:

$$P_4 k_z^4 + P_3 k_z^3 + P_2 k_z^2 + P_1 k_z + P_o = 0 \quad \text{(A5)}$$

where the polynomial coefficients are given by

$$P_4 = \omega_o^2 - \omega^2 + \Big(e_{nx}^2 + e_{ny}^2\Big)\omega_o\omega_m \quad \text{(A6)}$$

$$P_3 = -2e_{nz}\Big(e_{nx}k_x + e_{ny}k_y\Big)\omega_o\omega_m \quad \text{(A7)}$$

$$\begin{aligned} P_2 = {} & -2\Big(k_o^2 - k_x^2 - k_y^2\Big)\Big(\omega_o^2 + \omega_o\omega_m - \omega^2\Big) \\ & - \Big[k_o^2 - e_{nz}^2\Big(k_o^2 - k_x^2 - k_y^2\Big) + \Big(e_{nx}k_x + e_{ny}k_y\Big)^2\Big]\omega_o\omega_m \\ & - \Big(e_{nx}^2 + e_{ny}^2\Big)k_o^2\omega_m^2 \end{aligned} \quad \text{(A8)}$$

$$P_1 = 2e_{nz}\Big(e_{nx}k_x + e_{ny}k_y\Big)\omega_m\Big[k_o^2\omega_m + \Big(k_o^2 - k_x^2 - k_y^2\Big)\omega_o\Big] \quad \text{(A9)}$$

$$\underline{\underline{\mathbf{\Gamma}}}(z) = \begin{pmatrix} \zeta e_{Ax}\exp(ik_z z) & \zeta e_{Ax}\exp(-ik_z z) & \zeta e_{Bx}\exp(ik_z z) & \zeta e_{Bx}\exp(-ik_z z) \\ \zeta e_{Ay}\exp(ik_z z) & \zeta e_{Ay}\exp(-ik_z z) & \zeta e_{By}\exp(ik_z z) & \zeta e_{By}\exp(-ik_z z) \\ e_{Bx}\exp(ik_z z) & -e_{Bx}\exp(-ik_z z) & -e_{Ax}\exp(ik_z z) & e_{Ax}\exp(-ik_z z) \\ e_{By}\exp(ik_z z) & -e_{By}\exp(-ik_z z) & -e_{Ay}\exp(ik_z z) & e_{Ay}\exp(-ik_z z) \end{pmatrix} \quad \text{(A3)}$$

$$P_o = \left(k_o^2 - k_x^2 - k_y^2\right)\Big\{\left(k_o^2 - k_x^2 - k_y^2\right)\left(\omega_o^2 + \omega_o\omega_m - \omega^2\right) + \left[k_o^2 + (e_{nx}k_x + e_{ny}k_y)^2\right]\omega_o\omega_m + k_o^2\omega_m^2\Big\} + \left(e_{nx}k_x + e_{ny}k_y\right)^2 k_o^2\omega_m^2. \tag{A10}$$

Here, $\underline{\mathbf{e}}_n = (e_{nx}\ e_{ny}\ e_{nz})^T$ denotes the unit vector along the internal dc-bias field direction

$$k_o = \epsilon_f^{1/2}(\omega/c) \tag{A11}$$

$$\omega_m = 4\pi\gamma M_s \tag{A12}$$

$$\omega_o = \gamma H'_{\mathbf{in}}. \tag{A13}$$

ω is the angular frequency, γ is the gyromagnetic ratio, c is the speed of light in vacuum, ϵ_f is the dielectric constant of the ferrite, $4\pi M_s$ is the saturation magnetization, and $H'_{\mathbf{in}}$ is the effective internal bias magnetic field given by

$$H'_{\mathbf{in}} = H_o - 4\pi M_s N_z + H_A - i\Delta H \text{ for an easy axis} \tag{A14a}$$

$$H'_{\mathbf{in}} = \left[H_o(H_o + H_A)\right]^{1/2} - i\Delta H \text{ for an easy plane.} \tag{A14b}$$

Here, H_o denotes the externally applied dc magnetic field and ΔH is the FMR linewidth. In (A14a), the easy axis occurs along the z-axis and the anisotropy field is denoted as H_A [12, eq. (10)]. In (A14b), the easy plane lies on the xy-plane and the anisotropy field is H_A [12, eq. (6)]. For practical applications, H_o is applied along the easy-axis direction (the z-axis) or along a direction lying on the easy plane (the xy-plane). For the case of an easy axis, the demagnetizing field $4\pi M_s N_z$ needs to be subtracted from the total field, as expressed in (A14a). Here, N_z denotes the axial demagnetizing factor, which may be estimated from a static calculation [7]. For cubic ferrites (e.g., garnets), the anisotropy field is small, and the total internal effective field, $H'_{\mathbf{in}}$ is given by (A14a) assuming H_A is negligible. Magnetic loss is accounted for by the term $-i\Delta H$ in (A14a) and (A14b), and dielectric loss can be included by using the following complex dielectric constant:

$$\epsilon_f \to \epsilon_f(1 + i\tan\delta_f). \tag{A15}$$

In (A15), $\tan\delta_f$ denotes the dielectric loss tangent of the ferrite material.

After k_z's are solved from (A5), denoted as $k_{\alpha z}$, $\alpha = 1,2,3,4$, the magnetic permeability μ_α can be calculated from (4) as

$$\mu_\alpha = \left(k_x^2 + k_y^2 + k_{\alpha z}^2\right)\Big/k_o^2. \tag{A16}$$

The associated electromagnetic fields are, therefore,

$$\underline{\mathbf{h}}_\alpha = \underline{\underline{\mathbf{U}}}\,\underline{\mathbf{h}}_{\alpha'} \tag{A17}$$

$$\underline{\mathbf{e}}_\alpha = \underline{\underline{\mathbf{U}}}\,\underline{\mathbf{e}}_{\alpha'} \tag{A18}$$

$$\underline{\mathbf{b}}_\alpha = \underline{\underline{\mathbf{U}}}\,\underline{\mathbf{b}}_{\alpha'} \tag{A19}$$

where the primed fields are those expressed in a coordinate frame whose z-axis coincides with the internal dc-bias field direction [1]

$$h'_{\alpha x} = (i\omega/\gamma)\left(1 - \mu_\alpha\hat{e}_{\alpha 1}^2\right) + H'_{\mathbf{in}}\mu_\alpha\hat{e}_{\alpha 1}\hat{e}_{\alpha 2} \tag{A20}$$

$$h'_{\alpha y} = (-i\omega/\gamma)\mu_\alpha\hat{e}_{\alpha 1}\hat{e}_{\alpha 2} - H'_{\mathbf{in}}\left(1 - \mu_\alpha\hat{e}_{\alpha 2}^2\right) - 4\pi M_s\left[1 + \mu_\alpha\hat{e}_{\alpha 3}^2/(1 - \mu_\alpha)\right] \tag{A21}$$

$$h'_{\alpha z} = \hat{e}_{\alpha 3}\mu_\alpha\left\{(-i\omega/\gamma)\hat{e}_{\alpha 1} + \left[H'_{\mathbf{in}} + 4\pi M_s/(1 - \mu_\alpha)\right]\hat{e}_{\alpha 2}\right\} \tag{A22}$$

$$e'_{\alpha x} = -\zeta_\alpha\hat{e}_{\alpha 3}\left[H'_{\mathbf{in}} + 4\pi M_s(1 - \mu_\alpha\hat{e}_{\alpha 1}^2)/(1 - \mu_\alpha)\right] \tag{A23}$$

$$e'_{\alpha y} = \zeta_\alpha\hat{e}_{\alpha 3}\left[(-i\omega/\gamma) + 4\pi M_s\mu_\alpha\hat{e}_{\alpha 1}\hat{e}_{\alpha 2}/(1 - \mu_\alpha)\right] \tag{A24}$$

$$e'_{\alpha z} = \zeta_\alpha\Big\{H'_{\mathbf{in}}\hat{e}_{\alpha 1} + (i\omega/\gamma)\hat{e}_{\alpha 2} + 4\pi M_s\hat{e}_{\alpha 1} \cdot \left[1 + \mu_\alpha\hat{e}_{\alpha 3}^2/(1 - \mu_\alpha)\right]\Big\} \tag{A25}$$

$$b'_{\alpha x} = h'_{\alpha x} + (-i\omega/\gamma)(1 - \mu_\alpha) + 4\pi M_s\mu_\alpha\hat{e}_{\alpha 1}\hat{e}_{\alpha 2} \tag{A26}$$

$$b'_{\alpha y} = h'_{\alpha y} + H'_{\mathbf{in}}(1 - \mu_\alpha) + 4\pi M_s\left(1 - \mu_\alpha\hat{e}_{\alpha 1}^2\right) \tag{A27}$$

$$b'_{\alpha z} = h'_{\alpha z}. \tag{A28}$$

Here, $\hat{\mathbf{e}}_\alpha = (\hat{e}_{\alpha 1}\ \hat{e}_{\alpha 2}\ \hat{e}_{\alpha 3})^T$ denotes the unit vector along the wave propagation direction $\underline{\mathbf{k}}_\alpha = (k_x\ k_y\ k_{\alpha z})^T$, and $\zeta_\alpha = (\mu_\alpha/\epsilon_f)^{1/2}$ is the wave impedance. We note that for each mode α, the three vectors $\underline{\mathbf{e}}_\alpha$, $\underline{\mathbf{b}}_\alpha$, and $\underline{\mathbf{k}}_\alpha$ are mutually perpendicular to each other, as dictated by Maxwell equations. Also, $\underline{\mathbf{e}}_\alpha$ is perpendicular to $\underline{\mathbf{h}}_\alpha$, as can be readily verified. In (A17)–(A19), the coordinate transformation matrix $\underline{\underline{\mathbf{U}}}$ is given by (A29), shown at the top of the following page, and Θ and Φ denote the polar and azimuthal angles along the internal bias field direction. That is, $\underline{\mathbf{e}}_n = (\sin\Theta\cos\Phi,\ \sin\Theta\sin\Phi, \cos\Theta)^T$. Therefore, when $\underline{\mathbf{e}}_\alpha$, $\underline{\mathbf{h}}_\alpha$, and $\underline{\mathbf{k}}_\alpha$, $\alpha = 1,2,3,4$, are known from (A5), and from (A17)–(A29), the Γ-matrix of the ferrite layer can then be calculated using (2). The T-matrix can be calculated from the Γ-matrix by using (1).

REFERENCES

[1] B. Lax and K. J. Button, *Microwave Ferrites and Ferrimagnetics*. New York: McGraw-Hill, 1962.

[2] N. Alexópoulos, "Integrated-circuit structures on anisotropic substrates," *IEEE Trans. Microwave Theory Tech.*, vol. MTT-33, pp. 847–881, Oct. 1985.

[3] T. Q. Ho and B. Becker, "Frequency-dependent characteristics of shielded broadside coupled microstrip lines on anisotropic substrates," *IEEE Trans. Microwave Theory Tech.*, vol. 39, pp. 1021–1025, June 1991.

[4] G. W. Hanson, "A numerical formulation of dyadic Green's functions for planar bianisotropic media with application to printed transmission lines," *IEEE Trans. Microwave Theory Tech.*, vol. 44, pp. 144–151, Jan. 1996.

[5] M. R. Rosa, M. L. Albuquerque, A. G. D'Assumcio, R. G. Maia, and A. J. Giarola, "Full wave analysis of microstrip lines on ferrite and anisotropic dielectric substrate," *IEEE Trans. Magn.*, vol. 25, pp. 2944–2946, July 1989.

[6] E. L.-B. El-Sharawy and R. W. Jackson, "Coplanar waveguide and slot line on magnetic substrates: Analysis and experiment," *IEEE Trans. Microwave Theory Tech.*, vol. 36, pp. 1071–1079, June 1988.

$$\underline{\underline{U}} = \begin{pmatrix} 1-(1-\cos\Theta)\cos^2\Phi & -(1-\cos\Theta)\sin\Phi\cos\Phi & -\sin\Theta\cos\Phi \\ -(1-\cos\Theta)\sin\Phi\cos\Phi & 1-(1-\cos\Theta)\sin^2\Phi & -\sin\Theta\sin\Phi \\ \sin\Theta\cos\Phi & \sin\Theta\sin\Phi & \cos\Theta \end{pmatrix} \tag{A29}$$

[7] H. How, "Magnetic microwave devices," in *Encyclopedia of Electrical and Electronics Engineering*, J. G. Webster, Ed. New York: Wiley, 1999, vol. 12, pp. 31–45.

[8] H. How, P. Shi, C. Vittoria, E. Hokenson, M. H. Champion, L. C. Kempel, and K. D. Trott, "Steerable phased array antennas using single-crystal YIG phase shifters—Theory and experiments," *IEEE Trans. Microwave Theory Tech.*, vol. 48, pp. 1544–1549, Sept. 2000.

[9] D. M. Pozar, "Radiation and scattering characteristics of microstrip antennas on normally biased ferrite substrates," *IEEE Trans. Antennas Propagat.*, vol. 30, pp. 1084–1092, Sept. 1992.

[10] H. How, S. A. Oliver, S. W. McKnight, P. M. Zavracky, N. E. McGruer, and C. Vittoria, "Theory and experiment of thin-film junction circulator," *IEEE Trans. Microwave Theory Tech.*, vol. 46, pp. 1645–1653, Nov. 1998.

[11] W. H. Von Aulock, Ed., *Handbook of Microwave Ferrite Materials*. New York: Academic, 1965.

[12] H. How, X. Zuo, and C. Vittoria, "Electromagnetic wave propagation involving a magnetic easy plane," *IEEE Trans. Microwave Theory Tech.*, submitted for publication.

[13] N. Zeina, H. How, and C. Vittoria, "Self-biasing circulators operating at K_α-band utilizing M-type hexagonal ferrites," *IEEE Trans. Magn.*, vol. 28, pp. 3219–3221, Sept. 1992.

[14] A. Sommerfeld, *Partial Differential Equations*. New York: Academic, 1962.

[15] H. How, W. Tian, and C. Vittoria, "AC Hall effect in multilayered semiconductors," *J. Lightwave Technol.*, vol. 15, pp. 1006–1011, June 1997.

[16] H. How and C. Vittoria, "Microstrip antennas," in *Encyclopedia of Electrical and Electronics Engineering*, J. G. Webster, Ed. New York: Wiley, 2000, Suppl. I, pp. 349–366.

[17] H. How, L. C. Kempel, K. D. Trott, and C. Vittoria, "Green's function calculation on circular microstrip patch antennas," *IEEE Trans. Antennas Propagat.*, vol. 49, pp. 393–401, Mar. 2001.

[18] M. Hashimoto, "A rigorous solution for dispersive microstrip," *IEEE Trans. Microwave Theory Tech.*, vol. MTT-33, pp. 1131–1137, Nov. 1985.

[19] G. E. Forsythe, M. A. Malcolm, and C. B. Moler, *Computer Methods for Mathematical Computations*. Englewood Cliffs, NJ: Prentice-Hall, 1977.

Hoton How, photograph and biography not available at time of publication.

Xu Zuo, photograph and biography not available at time of publication.

Elwood Hokanson, photograph and biography not available at time of publication.

Leo C. Kempel (S'86–M'95–SM'99) was born in Akron, OH, in October 1965. He received the B.S.E.E. degree from the University of Cincinnati, Cincinnati, OH, in 1989, and the M.S.E.E. and Ph.D. degrees from The University of Michigan at Ann Arbor, in 1990 and 1994, respectively.

He participated in the University of Cincinnati's cooperative education program at General Dynamics/Fort Worth Division. After a brief Post-Doctoral appointment at The University of Michigan at Ann Arbor, he joined the Mission Research Corporation in 1994 as a Senior Research Engineer. He led several projects involving the design of conformal antennas, computational electromagnetics, scattering analysis, and high-power/ultra-wide-band microwaves. In 1998, he joined Michigan State University, East Lansing, as an Assistant Professor, where he currently conducts research in computational electromagnetics, teaches undergraduate and graduate courses in electromagnetics, and supervises the research of several M.S. and Ph.D. students. He co-authored *The Finite Element Method for Electromagnetics: Antennas, Microwave Circuits, and Scattering Applications* (Piscataway, NJ: IEEE Press, 1998). He is a reviewer for *JEWA* and *Radio Science*.

Dr. Kempel is a member of Tau Beta Pi, Eta Kappa Nu, and Commission B of the International Scientific Radio Union (URSI). He served as the Chapter IV vice-chair for the Southeast Michigan Chapter of the IEEE, as well as the technical chairperson for the 2001 ACES Conference. He has organized several sessions at recent URSI and ACES meetings. He is a reviewer for several IEEE publications.

Carmine Vittoria (S'62–M'63–SM'83–F'90), photograph and biography not available at time of publication.